

RESEARCH LETTER

10.1002/2015GL065395

Key Points:

- A statistical analysis is performed for SSW effects on the thermosphere
- A significant density reduction is revealed during SSWs
- We suggest wave forcing from the lower atmosphere as a possible mechanism

Supporting Information:

- Table S1 and Figure S1

Correspondence to:

Y. Yamazaki,
y.yamazaki@lancaster.ac.uk

Citation:

Yamazaki, Y., M. J. Kosch, and J. T. Emmert (2015), Evidence for stratospheric sudden warming effects on the upper thermosphere derived from satellite orbital decay data during 1967–2013, *Geophys. Res. Lett.*, 42, doi:10.1002/2015GL065395.

Received 15 JUL 2015

Accepted 27 JUL 2015

Accepted article online 29 JUL 2015

©2015. The Authors.

This is an open access article under the terms of the Creative Commons Attribution License, which permits use, distribution and reproduction in any medium, provided the original work is properly cited.

Evidence for stratospheric sudden warming effects on the upper thermosphere derived from satellite orbital decay data during 1967–2013

Yosuke Yamazaki¹, Michael J. Kosch^{1,2}, and John T. Emmert³

¹Department of Physics, Lancaster University, Lancaster, UK, ²South African National Space Agency, Hermanus, South Africa, ³Space Science Division, U.S. Naval Research Laboratory, Washington, District of Columbia, USA

Abstract We investigate possible impact of stratospheric sudden warmings (SSWs) on the thermosphere by using long-term data of the global average thermospheric total mass density derived from satellite orbital drag during 1967–2013. Residuals are analyzed between the data and empirical Global Average Mass Density Model (GAMDM) that takes into account density variability due to solar activity, season, geomagnetic activity, and long-term trend. A superposed epoch analysis of 37 SSW events reveals a density reduction of 3–7% at 250–575 km around the time of maximum polar vortex weakening. The relative density perturbation is found to be greater at higher altitudes. The temperature perturbation is estimated to be -7.0 K at 400 km. We show that the density reduction can arise from enhanced wave forcing from the lower atmosphere.

1. Introduction

A stratospheric sudden warming (SSW) is a large-scale meteorological disturbance that usually takes place in the arctic region during winter [e.g., *Andrews et al.*, 1987]. Upward propagation of planetary waves transfers energy and momentum from the troposphere to the stratosphere to initiate the disturbance [*Matsuno*, 1971]. An SSW significantly alters the mean state of the middle atmosphere [*Liu and Roble*, 2002], which in turn affects the propagation of other atmospheric waves into the upper atmosphere [*Stening et al.*, 1997; *Liu et al.*, 2010].

Ionospheric effects during SSW events have been recognized in recent years, especially in the wake of an unusually strong and prolonged SSW event in January 2009 [*Manney et al.*, 2009]. Studies found marked changes in the plasma density at low latitudes [e.g., *Chau et al.*, 2010; *Goncharenko et al.*, 2010]. These ionospheric modulations have been attributed mainly to electrodynamic effects induced by enhanced semidiurnal tidal waves [e.g., *Jin et al.*, 2012; *Wang et al.*, 2014].

In contrast to the successful progress in the understanding of ionospheric effects during SSWs, it has been controversial whether an SSW has any measurable impact on the thermosphere. Unlike the ionosphere, remote sensing of the thermosphere is difficult, and available data are very limited. Using satellite-borne accelerometer data, *Liu et al.* [2011] suggested that the thermospheric density at 325–475 km underwent an anomalous decrease of 30–45% during the January 2009 SSW. This claim was, however, immediately questioned by *Fuller-Rowell et al.* [2011], who showed that the apparent density reduction reported by *Liu et al.* [2011] can be largely explained by changes in geomagnetic activity. It was therefore concluded that there was no evidence of thermospheric effects during the January 2009 SSW. *Conde and Nicolls* [2010], examining temperature data at 240 km for the same event, also noted difficulties in separating contributions of the SSW from other sources.

Another issue regarding possible SSW impact on the thermosphere is the lack of a consensus among predictions by general circulation models. *Pedatella et al.* [2014a] compared simulation results for the January 2009 SSW event obtained from these whole atmosphere models: GAIA [*Jin et al.*, 2011], HAMMONIA [*Schmidt et al.*, 2006], WAM [*Fuller-Rowell et al.*, 2010], and WACCM-X [*Liu*, 2014]. The comparison revealed that although the models show reasonable agreement in the troposphere and stratosphere, the model results become diverse as the altitude increases and have significant discrepancies in the thermosphere. Therefore, there is no reliable prediction at present about how the thermosphere would respond to SSWs and how much the effect would be.

In this study, we use long-term records of the global average thermospheric density derived from satellite orbital decay data, which for the first time make it possible to investigate the thermospheric response to SSW events in a statistical way. The results reveal a global reduction in upper thermospheric density during SSWs. We suggest enhanced wave forcing from below as a possible cause for the density reduction. We use the thermosphere-ionosphere-electrodynamics general circulation model (TIE-GCM) [Richmond *et al.*, 1992] to demonstrate how wave forcing would affect the upper thermosphere.

2. Data and Models

The height-dependent, global average density data set we use was detailed by Emmert [2009, 2015]. Briefly, the decay rates of the mean orbital period of near-Earth orbit satellites are proportional to the total mass density along the orbital track. This relationship can be used to evaluate the thermospheric density from orbital trajectory data. The use of historical orbital records enables construction of long time series. Combining densities from multiple objects, it is possible to obtain a representation of the global average density, but with a limited temporal resolution. The data set constructed by Emmert [2015] incorporates orbital data from ~5000 objects. It covers the period from January 1967 to December 2013 and altitudes between 250 and 575 km. Estimated daily relative accuracy is ~2%, and estimated absolute accuracy is ~10% [Emmert, 2009, section 4]. Although we use daily data, the maximum temporal resolution is 3 days because of 3 day cubic spline smoothing involved in the density retrieval procedure [Emmert, 2009, section 7]. The reader is referred to Emmert [2009] for further information on the derivation of the global average mass density and error evaluation.

The Global Average Mass Density Model (GAMDM) is an empirical model of global daily average thermospheric density, which was constructed on the basis of function fits to the density product described in the previous paragraph. Emmert and Picone [2010] discussed the construction details of GAMDM. The model uses solar activity index $F_{10.7}$, geomagnetic activity index Kp , and day of year as input parameters to evaluate contributions of solar and geomagnetic activity, and season. The residuals between the data and GAMDM may be interpreted as resulting from other sources, such as increasing CO_2 concentration [Emmert *et al.*, 2008]. The latest version of GAMDM, which we use, takes into account the effect of the CO_2 increase [Emmert *et al.*, 2014; Emmert, 2015]. Since GAMDM does not include any forcing term associated with SSWs, the effect of SSWs on the thermospheric density, if there is any, would lead to overestimation or underestimation of the model prediction in comparison with the data. As reported by Emmert *et al.* [2014], the density data during 2006–2010 were consistently lower than GAMDM predictions, by up to 20% on average at 400 km [Emmert, 2015, Figure 2c]. In addition, the 400 km residuals have an interannual variance of ~3% [Emmert *et al.*, 2014, Table 5]. Since these annual-scale anomalies are presumably unrelated to shorter-term SSW events, we remove them by subtracting running annual averages of the residuals from the residual time series prior to conducting our analysis.

Different studies have used different criteria for the detection of SSWs [Butler *et al.*, 2015]. One of the most commonly used diagnostics is the zonal mean zonal wind at 60° and 10 hPa (~32 km), which has been found useful in studies of stratosphere-troposphere coupling [e.g., Charlton and Polvani, 2007]. For upper atmospheric studies, Zhang and Forbes [2014] and Chau *et al.* [2015] used the zonal mean zonal wind at 70° at 1 hPa (~48 km) to find a remarkable correlation between the polar vortex weakening and semidiurnal lunar tidal activity in the lower thermosphere, in terms of both timing and intensity. The success of the use of zonal wind at 1 hPa, instead of 10 hPa, probably reflects the fact that a breakdown or weakening of the polar vortex begins at an altitude higher than 10 hPa and gradually descends to lower levels. In this study, we also use the zonal mean zonal wind at 70° at 1 hPa to identify SSWs. Wind and temperature data were obtained from global meteorological reanalysis produced by the European Centre for Medium-Range Weather Forecasts (ECMWF). Specifically, we use ERA-Interim [Dee *et al.*, 2011] for 1979–2014 and ERA-40 [Uppala *et al.*, 2005] for 1966–1978.

The TIE-GCM is a first-principles model of the coupled thermosphere-ionosphere system [Richmond *et al.*, 1992; Qian *et al.*, 2014]. It solves the continuity, momentum, and energy equations with self-consistent electrostatics over a height range from approximately 96 km to 600 km. For the present study, we use version 1.95 of the TIE-GCM. The model resolution is 5° in latitude and 5° in longitude with two grid points per scale height. Tidal forcing at the lower boundary was specified for migrating diurnal and semidiurnal tides

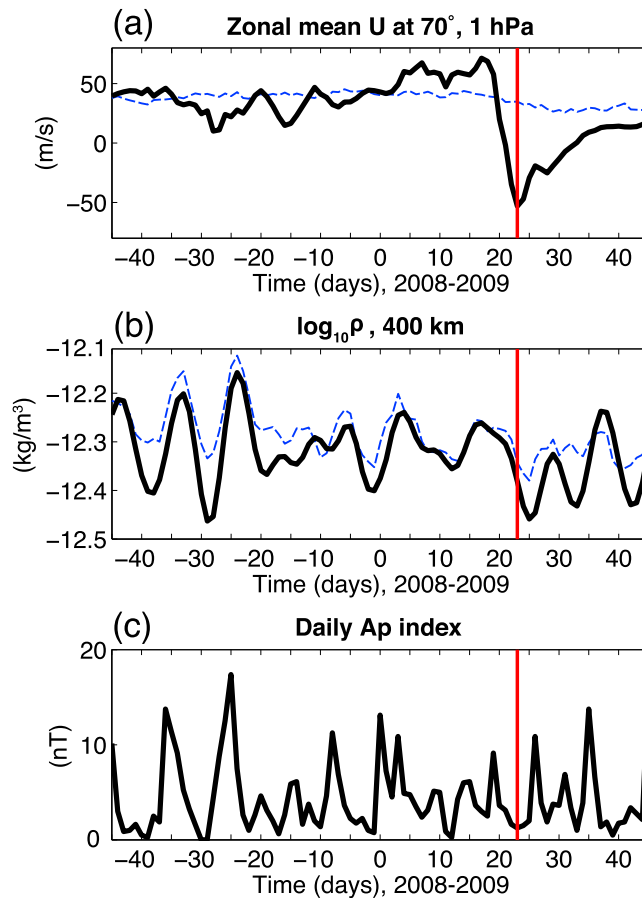


Figure 1. The January 2009 SSW event. (a) Zonal mean zonal wind at 70°N latitude at 1 hPa (~48 km). The solid line shows the daily data, and the dashed line shows the climatological median for the period 1966–2014. (b) Logarithm (base 10) of global average thermospheric total mass density at 400 km. The solid line shows the daily data, and the dashed line shows the GAMDM predictions. (c) Geomagnetic activity index A_p . The vertical red lines indicate the day of the peak polar vortex weakening.

using the Global Scale Wave Model (GSWM) [Hagan and Forbes, 2002, 2003]. Also, eddy diffusivity at the lower boundary was specified in the way described by Qian *et al.* [2009].

3. Results

3.1. Case Study: January 2009 SSW Event

We first present the thermospheric density variability during the January 2009 SSW event. Figure 1a depicts the zonal mean zonal wind at 70°N at 1 hPa. The solid line shows the wind for the winter period of 2008–2009, while the dashed line shows the climatological median derived from the daily data during 1966–2014. A reduction of the zonal mean zonal wind from the climatological median is evident around day 20–30, indicating significant weakening of the polar vortex, and hence the occurrence of SSW. We plot in Figure 1b the thermospheric density at 400 km for the corresponding period. The results from the data and GAMDM are shown by the black and blue lines, respectively. It can be seen that GAMDM captures most of the density variability. Some of the changes are clearly correlated with changes in geomagnetic activity, which is shown in Figure 1c. GAMDM overestimates the density around the SSW event, especially after the peak polar vortex weakening. The maximum discrepancy occurred on day 25, when the data-GAMDM residual was –7% (after the annual average was removed from the residual time series).

It is obviously arguable if the density reduction around day 25 is actually associated with the SSW event. One can see in Figure 1b that GAMDM similarly overestimates the density around day –40 and day –30 without SSW. According to Emmert *et al.* [2014, Table 5], the day-to-day variability (standard deviation) of the GAMDM residuals is ~13% at 400 km. Therefore, the density reduction of 7% is smaller than the background noise.

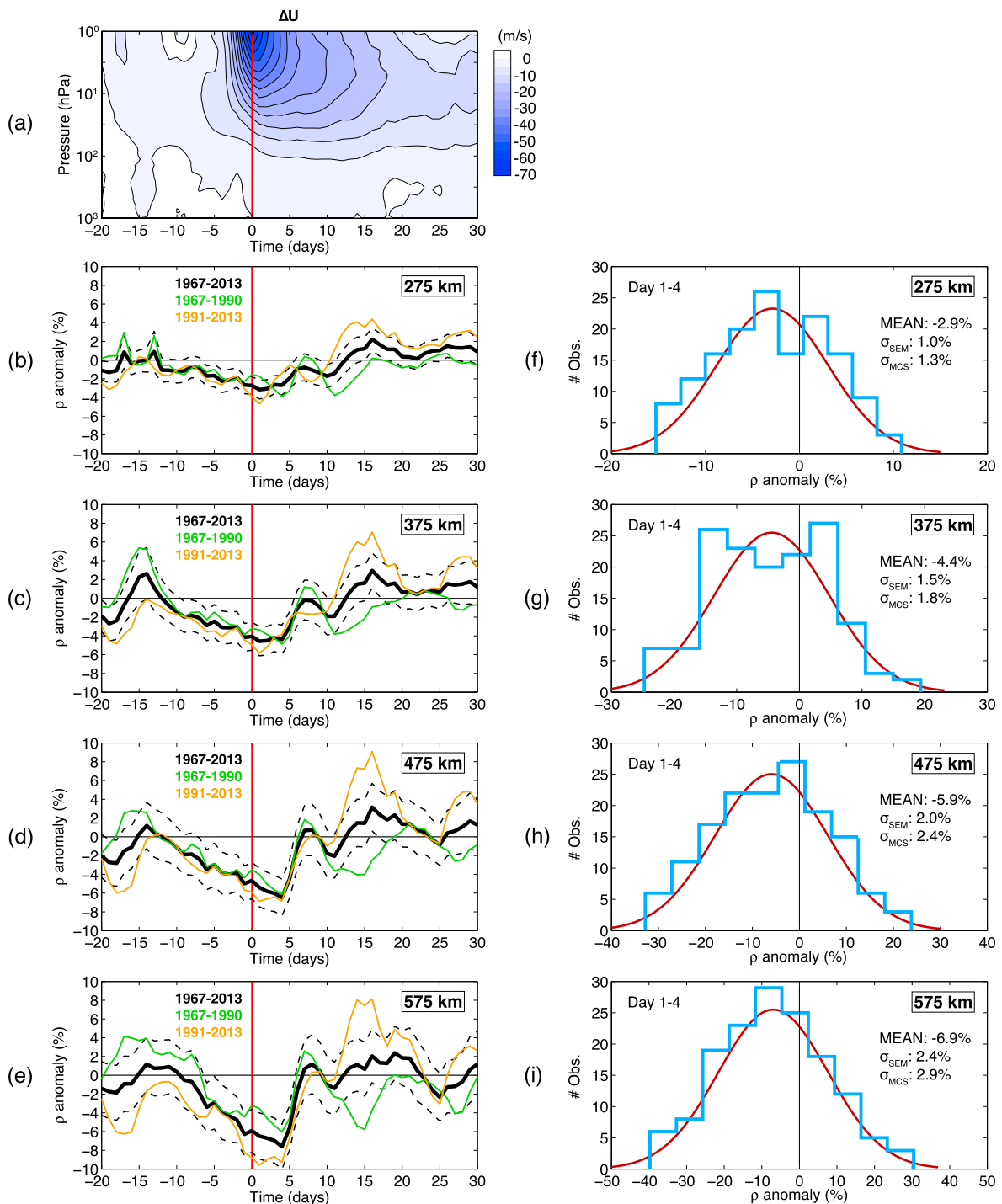


Figure 2. Results for a superposed epoch analysis for 37 SSW events during 1967–2013. (a) Average zonal mean zonal wind anomaly at 70°N latitude. (b–e) Average thermospheric total mass density anomalies at 275, 375, 475, and 575 km. The black lines show the results for 1967–2013; the dotted lines show the corresponding standard error of the mean (SEM). The green and orange lines show the results for 1967–1990 and for 1991–2013, respectively. (f–i) Distribution of the density anomaly for day 1–4 (blue histogram), and the corresponding Gaussian distribution (red curve). The mean value, along with the estimated 1σ uncertainty by SEM (σ_{SEM}) and by a Monte Carlo simulation (σ_{MCS}) are also indicated.

Our investigation of other individual SSW events also encountered difficulties in separating possible SSW signals from the large noise. We thus choose not to conclude about SSW effects on the thermospheric density from individual events. Instead, we take a statistical approach that reduces the noise, as described in the next section.

3.2. Superposed Epoch Analysis

A superposed epoch analysis is a statistical analysis technique, widely used in geophysical research, to estimate the characteristic response of a system to a type of event [e.g., *Fejer et al.*, 2002; *Bristow and Jensen*, 2007]. We employed the technique to estimate the average response of thermospheric density perturbation to SSW events during 1967–2013. An SSW event was identified when the daily mean value of the zonal mean zonal wind at 70° and 1 hPa was below the climatological median by more than 20 m/s for at least three consecutive days. We focused on the Northern Hemisphere mid winter period, defined here as ± 45 days from the first day of the year. Once an SSW event was detected, the day for the peak polar vortex weakening (i.e., minimum zonal mean zonal wind) was assigned as “day 0,” and no event was considered for the following 30 days. We found 37 SSW events during the period examined, which leads to the occurrence rate of 0.79 events per winter, in agreement with the results from other SSW definitions in the literature [e.g., *Butler et al.*, 2015]. A list of the 37 SSW events is given in the supporting information.

Figure 2a shows the average of the wind anomaly for the 37 SSW events. The westward wind anomaly starts to develop 5–10 days before the peak polar vortex weakening. As the altitude increases, the magnitude of the westward wind anomaly becomes greater, and the peak of polar vortex weakening occurs earlier. After the peak polar vortex weakening, the wind gradually recovers to the normal level in 20–25 days at 1 hPa.

In Figures 2b–2e, the black lines depict the average of the density anomaly for the 37 SSW events at 275, 375, 475, and 575 km. Similar plots showing the density anomaly for all 37 individual SSW events can be found in the supporting information. The average signal reveals a reduction of the thermospheric density during SSWs at all heights. The maximum density reduction occurs 1–4 days after the peak polar vortex weakening. The relative density perturbation during SSWs is greater at higher altitudes.

Figures 2f–2i display the distribution of the density anomaly for days 1–4. The average density perturbations are -2.9% , -4.4% , -5.9% , and -6.9% at 275, 375, 475, and 575 km, respectively. The density anomaly has an approximately Gaussian distribution, especially at 475 and 575 km. The 1σ uncertainty of the mean may be estimated to be the standard error of the mean (SEM), i.e., the standard deviation of the sample divided by the square root of the number of the independent samples (i.e., 37). The calculated 1σ uncertainty estimates are 1.0%, 1.5%, 2.0%, and 2.4% at 275, 375, 475, and 575 km, respectively. It is noted that these uncertainty estimates relate to the mean for the 37 SSW events, not individual events. In order to ensure that these uncertainty estimates are reasonable, the 1σ uncertainty of the mean was also evaluated using a Monte Carlo simulation. We selected 37 random epochs in the data set and calculated the average density anomaly. This procedure was repeated 2000 times. The standard deviation of these 2000 mean values was computed as the estimated 1σ uncertainty. It is noted that the standard deviation of the data-GAMDM residuals do not depend on solar activity, season, or geomagnetic activity [*Emmert and Picone*, 2010, Figure 10]. The derived 1σ uncertainties are 1.3%, 1.8%, 2.4%, and 2.9%, which is largely consistent with the SEMs. Thus, the deviation of the average density perturbation during SSWs is larger than the estimated 2σ uncertainty of the mean at all heights.

We also compared the average density perturbation for the first 19 SSW events with that for the last 18 events, which are plotted in Figures 2b–2e by the green and orange lines, respectively. The pattern is remarkably consistent between days -15 and 7, with the maximum negative response near the peak polar vortex weakening. The consistency between the two halves of the data set gives us further confidence that the density reduction during SSWs is physically meaningful.

4. Discussion

4.1. Temperature Response

Simulations and observations have indicated significant temperature changes in the polar middle atmosphere during SSWs [e.g., *Liu and Roble*, 2002; *Funke et al.*, 2010]. These studies showed mesospheric cooling (70–90 km) and lower thermospheric warming (120–140 km), along with stratospheric warming (30–50 km). However, little is known about how the thermospheric temperature changes on a global scale during SSWs. *Liu et al.* [2013, 2014] reported a long-term decrease (~ 30 days) in the global average temperature by -12 K for the January 2009 event using GAIA. There has been no observational evidence to verify the results.

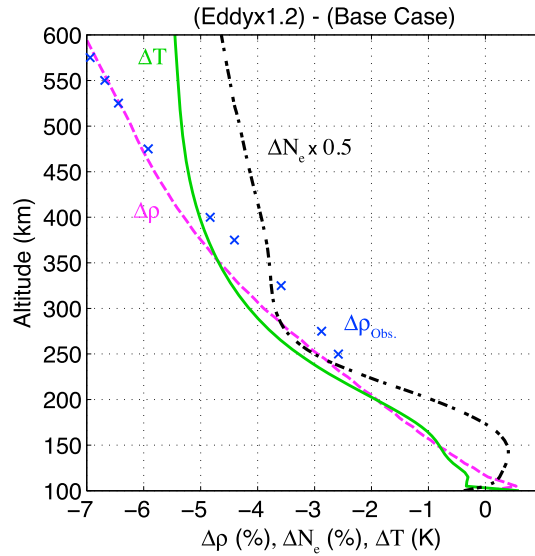


Figure 3. Height dependence of the thermospheric total mass density anomaly during SSWs averaged over days 1–4 (blue crosses). Results for the TIE-GCM numerical experiment are also shown; changes in the global mean total mass density (magenta dashed line), temperature (green solid line), and one half the plasma density (black dash-dotted line) due to elevated eddy diffusivity at the lower boundary. The plasma density values were scaled for better display.

the NRLMSISE-00 model [Picone *et al.*, 2002], $T = 930$ K, and $M = 16.1$ amu for solar activity index $F_{10.7} = 135$ solar flux unit ($1 \text{ sfu} = 10^{-22} \text{ W m}^{-2} \text{ Hz}^{-1}$) and geomagnetic activity index $Ap = 12$ nT. These $F_{10.7}$ and Ap values correspond to the average values for the data analysis presented in section 3.2. At 400 km, $g = 8.68 \text{ m s}^{-2}$. Thus, ΔT is -7.0 ± 2.5 K, where the 1σ uncertainty was derived from the estimated 1σ uncertainty in the vertical gradient of the density perturbation. The actual 1σ error in the temperature perturbation may be greater as we did not take into account errors in T and M . Our estimate for the temperature perturbation is similar to but somewhat smaller than the 12 K reduction predicted by Liu *et al.* [2013, 2014] for the January 2009 event using GAIA.

4.2. Mechanism for Density Reduction

Changes in the thermospheric density at a fixed altitude can arise from changes in both temperature and composition [e.g., Lei *et al.*, 2010]. The mechanism we focus on in this study is wave forcing from below the thermosphere. The dissipation of upward propagating gravity waves in the mesosphere and lower thermosphere induces a downward transfer of heat, which causes cooling at the higher levels [Walterscheid, 1981; Akmaev, 2007]. Cooling at a given height of the thermosphere would lead to a reduction of the density in the region above owing to the contraction of the air. Besides, breakdown of gravity waves generates diffusive turbulence [Lindzen, 1981], which induces a downward transport of atomic oxygen O. Since the atomic oxygen is the major constituent of the thermosphere at 250–575 km, the loss of O due to the downward transport means a reduction of the total mass density.

Figure 3 illustrates the effect of enhanced gravity wave dissipation in the lower thermosphere. We performed two TIE-GCM simulations. A “Base Case” simulation was run for steady state 1 January conditions with $F_{10.7} = 135$ sfu and $Ap = 12$ nT, and the other simulation was run with the same model configuration except that the eddy diffusivity at the model lower boundary (~ 96 km) was increased by 20%. We calculated the global mean of total mass density, temperature, and plasma density for each run. Plotted in Figure 3 are the differences. The modulation of the eddy diffusivity at the TIE-GCM lower boundary has been used in previous studies to evaluate the effect of gravity wave forcing on the thermosphere-ionosphere system [e.g., Qian *et al.*, 2009, 2013]. The results in Figure 3 reveal a reduction in the global mean density, similar to observations during SSWs. It is known that changes in the background wind during SSWs significantly influence upward propagation of gravity waves. Studies have shown enhanced gravity wave forcing during

Here, we estimate the change in the global average temperature during SSWs from the height gradient of the density perturbation. Under hydrostatic equilibrium, the mass density ρ is related to temperature T and mean molecular mass M by

$$\frac{d}{dz} \ln \rho = -\frac{Mg}{kT} - \frac{d}{dz} \ln T + \frac{d}{dz} \ln M \quad (1)$$

where z is height, g is the acceleration due to gravity, and k is Boltzmann constant ($= 1.38 \times 10^{-23} \text{ J/K}$). At 400 km, the gradients in T and M are small and can be neglected. Also ignoring perturbations in M , the perturbed equation is

$$\Delta \left(\frac{d}{dz} \ln \rho \right) \approx \frac{d}{dz} \left(\frac{\Delta \rho}{\rho} \right) \approx \frac{Mg}{kT^2} \Delta T \quad (2)$$

so that

$$\Delta T \approx \frac{kT^2}{Mg} \frac{d}{dz} \left(\frac{\Delta \rho}{\rho} \right) \quad (3)$$

In Figure 3, the blue crosses show the height dependence of the density perturbation at 250–575 km during SSWs (days 1–4). From the figure, $\frac{d}{dz} \left(\frac{\Delta \rho}{\rho} \right) \approx -1.37 \times 10^{-7} \text{ m}^{-1}$, and from

the developing phase of SSWs [e.g., Hoffmann et al., 2007; Yamashita et al., 2010; Yiğit and Medvedev, 2012]. Although it is not known how the eddy diffusivity changes in the mesosphere and lower thermosphere during SSWs, the short-term change of 20% seems plausible given that the eddy diffusivity varies (locally, at least) by a factor of 3 or so on the seasonal time scale [Kirchhoff and Clemesha, 1983; Fukao et al., 1994; Sasi and Vijayan, 2001].

SSWs also affect upward propagation of various tides and planetary waves [e.g., Pedatella et al., 2014a]. Particularly, the solar migrating semidiurnal tide has been reported to exhibit significant amplification during SSWs [e.g., Wang et al., 2012; Pedatella et al., 2014b]. The dissipation of upward propagating tides in the mesosphere and lower thermosphere is known to have an effect similar to that achieved by increasing eddy diffusivity [e.g., Akmaev and Shved, 1980; Forbes et al., 1993]. Our TIE-GCM experiment revealed that the results similar to Figure 3 can be obtained by increasing the amplitude of the solar migrating semidiurnal tide at the lower boundary by a factor of 3 (not shown). TIE-GCM experiments of this kind have been used in previous studies for the assessment of the thermospheric response to tidal forcing from below [e.g., Yamazaki and Richmond, 2013; Jones et al., 2014].

As shown in Figures 3, the enhanced wave forcing brings about a decrease in the *F* region plasma density. This is because the loss of O reduces the production of O⁺ that dominates the *F* region plasma population. Satellite observations during the January 2009 SSW revealed a global-scale reduction in the electron density [Pancheva and Mukhtarov, 2011; Lin et al., 2012].

Although we have shown that enhanced wave forcing can induce a reduction of the global mean thermospheric density similar to observations during SSWs, it is open to question what waves would play a significant role and how important this mechanism would be relative to other mechanisms. Other possible mechanisms include cooling and shrinking of the mesosphere, which would lead to a reduction of the thermospheric density at a fixed altitude. At high latitudes, SSWs are often accompanied by cooling in the mesosphere. However, the region of the strong cooling is mostly confined to the Arctic region and the impact on the global mean density is expected to be marginal. Cooling/heating in the tropical mesosphere during SSWs is not well established, and its possible impact on the global mean thermospheric density is yet to be studied.

Acknowledgments

The magnetic index *A_p* was provided by the German Research Center for Geosciences (GFZ). The solar activity index *F*_{10.7} was provided by the Herzberg Institute of Astrophysics. ERA-Interim and ERA-40 reanalyses are available at the ECMWF website (<http://www.ecmwf.int/>). The thermospheric density data and GAMDM values are available in the supporting information of Emmert [2015]. The TIE-GCM (version 1.95) is available at the website (<http://www.hao.ucar.edu/modeling/tgcm/tiegcm1.95/>). The numerical data for the data analysis and simulation results will be made available upon request. This work was made when Y.Y. was a visiting scientist at the University of Colorado, Boulder. Y.Y. gratefully acknowledges useful discussion with Jeffrey Thayer, and Vicki Hsu. Y.Y. and M.J.K. were supported by NERC grant NE/K01207X/1. J.T.E. was supported by the Chief of Naval Research.

The Editor thanks two anonymous reviewers for their assistance in evaluating this paper.

References

- Akmaev, R. A. (2007), On the energetics of mean-flow interactions with thermally dissipating gravity waves, *J. Geophys. Res.*, *112*, D11125, doi:10.1029/2006JD007908.
- Akmaev, R. A., and G. M. Shved (1980), Modelling of the composition of the lower thermosphere taking account of the dynamics with applications to tidal variations of the [OI] 5577 Å airglow, *J. Atmos. Terr. Phys.*, *42*, 705–716.
- Andrews, D., J. R. Holton, and C. B. Leovy (1987), *Middle Atmosphere Dynamics*, pp. 259–294, Elsevier, New York.
- Bristow, W. A., and P. Jensen (2007), A superposed epoch study of SuperDARN convection observations during substorms, *J. Geophys. Res.*, *112*, A06232, doi:10.1029/2006JA012049.
- Butler, A., D. Seidel, S. Hardiman, N. Butchart, T. Birner, and A. Match (2015), Defining sudden stratospheric warmings, *Bull. Am. Meteorol. Soc.*, doi:10.1175/BAMS-D-13-00173.1, in press.
- Charlton, A., and L. M. Polvani (2007), A new look at stratospheric sudden warmings. Part I: Climatology and modeling benchmarks, *J. Clim.*, *20*, 449–469, doi:10.1175/JCLI3996.1.
- Chau, J. L., N. A. Aponte, E. Cabassa, M. P. Sulzer, L. P. Goncharenko, and S. A. González (2010), Quiet time ionospheric variability over Arecibo during sudden stratospheric warming events, *J. Geophys. Res.*, *115*, A00G06, doi:10.1029/2010JA015378.
- Chau, J. L., P. Hoffmann, N. M. Pedatella, V. Matthias, and G. Stober (2015), Upper mesospheric lunar tides over middle and high latitudes during sudden stratospheric warming events, *J. Geophys. Res. Space Physics*, *120*, 3084–3096, doi:10.1002/2015JA020998.
- Conde, M. G., and M. J. Nicolls (2010), Thermospheric temperatures above Poker Flat, Alaska, during the stratospheric warming event of January and February 2009, *J. Geophys. Res.*, *115*, D00N05, doi:10.1029/2010JD014280.
- Dee, D. P., et al. (2011), The ERA-Interim reanalysis: Configuration and performance of the data assimilation system, *Q. J. R. Meteorol. Soc.*, *137*, 553–597.
- Emmert, J. T. (2009), A long-term data set of globally averaged thermospheric total mass density, *J. Geophys. Res.*, *114*, A06315, doi:10.1029/2009JA014102.
- Emmert, J. T. (2015), Altitude and solar activity dependence of 1967–2005 thermospheric density trends derived from orbital drag, *J. Geophys. Res. Space Physics*, *120*, 2940–2950, doi:10.1002/2015JA021047.
- Emmert, J. T., and J. M. Picone (2010), Climatology of globally averaged thermospheric mass density, *J. Geophys. Res.*, *115*, A09326, doi:10.1029/2010JA015298.
- Emmert, J. T., J. M. Picone, and R. R. Meier (2008), Thermospheric global average density trends, 1967–2007, derived from orbits of 5000 near-Earth objects, *Geophys. Res. Lett.*, *35*, L05101, doi:10.1029/2007GL032809.
- Emmert, J. T., S. E. McDonald, D. P. Drob, R. R. Meier, J. L. Lean, and J. M. Picone (2014), Attribution of interminima changes in the global thermosphere and ionosphere, *J. Geophys. Res. Space Physics*, *119*, 6657–6688, doi:10.1002/2013JA019484.
- Fejer, B. G., J. T. Emmert, and D. P. Sipler (2002), Climatology and storm time dependence of nighttime thermospheric neutral winds over Millstone Hill, *J. Geophys. Res.*, *107*(A5), 1052, doi:10.1029/2001JA000300.
- Forbes, J. M., R. G. Roble, and C. G. Fesen (1993), Acceleration, heating, and compositional mixing of the thermosphere due to upward propagating tides, *J. Geophys. Res.*, *98*(A1), 311–321, doi:10.1029/92JA00442.

- Fukao, S., M. D. Yamanaka, N. Ao, W. K. Hocking, T. Sato, M. Yamamoto, T. Nakamura, T. Tsuda, and S. Kato (1994), Seasonal variability of vertical eddy diffusivity in the middle atmosphere: 1. Three-year observations by the middle and upper atmosphere radar, *J. Geophys. Res.*, *99*(D9), 18,973–18,987, doi:10.1029/94JD00911.
- Fuller-Rowell, T., F. Wu, R. Akmaev, T. -W. Fang, and E. Araujo-Pradere (2010), A whole atmosphere model simulation of the impact of a sudden stratospheric warming on thermosphere dynamics and electrodynamics, *J. Geophys. Res.*, *115*, A00G08, doi:10.1029/2010JA015524.
- Fuller-Rowell, T., R. Akmaev, F. Wu, M. Fedrizzi, R. A. Viereck, and H. Wang (2011), Did the January 2009 sudden stratospheric warming cool or warm the thermosphere?, *Geophys. Res. Lett.*, *38*, L18104, doi:10.1029/2011GL048985.
- Funke, B., M. López-Puertas, D. Bermejo-Pantaleón, M. García-Comas, G. P. Stiller, T. von Clarmann, M. Kiefer, and A. Linden (2010), Evidence for dynamical coupling from the lower atmosphere to the thermosphere during a major stratospheric warming, *Geophys. Res. Lett.*, *37*, L13803, doi:10.1029/2010GL043619.
- Goncharenko, L. P., A. J. Coster, J. L. Chau, and C. E. Valladares (2010), Impact of sudden stratospheric warmings on equatorial ionization anomaly, *J. Geophys. Res.*, *115*, A00G07, doi:10.1029/2010JA015400.
- Hagan, M. E., and J. M. Forbes (2002), Migrating and nonmigrating diurnal tides in the middle and upper atmosphere excited by tropospheric latent heat release, *J. Geophys. Res.*, *107*(D24), 4754, doi:10.1029/2001JD001236.
- Hagan, M. E., and J. M. Forbes (2003), Migrating and nonmigrating semidiurnal tides in the upper atmosphere excited by tropospheric latent heat release, *J. Geophys. Res.*, *108*(A2), 1062, doi:10.1029/2002JA009466.
- Hoffmann, P., W. Singer, D. Keuer, W. K. Hocking, M. Kunze, and Y. Murayama (2007), Latitudinal and longitudinal variability of mesospheric winds and temperatures during stratospheric warming events, *J. Atmos. Sol. Terr. Phys.*, *69*, 2355–2366.
- Jin, H., Y. Miyoshi, H. Fujiwara, H. Shinagawa, K. Terada, N. Terada, M. Ishii, Y. Otsuka, and A. Saito (2011), Vertical connection from the tropospheric activities to the ionospheric longitudinal structure simulated by a new Earth's whole atmosphere-ionosphere coupled model, *J. Geophys. Res.*, *116*, A01316, doi:10.1029/2010JA015925.
- Jin, H., Y. Miyoshi, D. Pancheva, P. Mukhtarov, H. Fujiwara, and H. Shinagawa (2012), Response of migrating tides to the stratospheric sudden warming in 2009 and their effects on the ionosphere studied by a whole atmosphere-ionosphere model GAIA with COSMIC and TIMED/SABER observations, *J. Geophys. Res.*, *117*, A10323, doi:10.1029/2012JA017650.
- Jones, M., Jr., J. M. Forbes, M. E. Hagan, and A. Maute (2014), Impacts of vertically propagating tides on the mean state of the ionosphere-thermosphere system, *J. Geophys. Res. Space Physics*, *119*, 2197–2213, doi:10.1002/2013JA019744.
- Kirchhoff, V. W. J. H., and B. R. Clemesha (1983), Eddy diffusion coefficients in the lower thermosphere, *J. Geophys. Res.*, *88*(A7), 5765–5768, doi:10.1029/JA088iA07p05765.
- Lei, J., J. P. Thayer, A. G. Burns, G. Lu, and Y. Deng (2010), Wind and temperature effects on thermosphere mass density response to the November 2004 geomagnetic storm, *J. Geophys. Res.*, *115*, A05303, doi:10.1029/2009JA014754.
- Lin, J. T., C. H. Lin, L. C. Chang, H. H. Huang, J. Y. Liu, A. B. Chen, C. H. Chen, and C. H. Liu (2012), Observational evidence of ionospheric migrating tide modification during the 2009 stratospheric sudden warming, *Geophys. Res. Lett.*, *39*, L02101, doi:10.1029/2011GL050248.
- Lindzen, R. S. (1981), Turbulence and stress owing to gravity wave and tidal breakdown, *J. Geophys. Res.*, *86*(C10), 9707–9714, doi:10.1029/JC086iC10p09707.
- Liu, H., and R. G. Roble (2002), A study of a self-generated stratospheric sudden warming and its mesospheric-lower thermospheric impacts using the coupled TIME-GCM/CCM3, *J. Geophys. Res.*, *107*(D23), 4695, doi:10.1029/2001JD001533.
- Liu, H., E. Doornbos, M. Yamamoto, and S. Tulasi Ram (2011), Strong thermospheric cooling during the 2009 major stratosphere warming, *Geophys. Res. Lett.*, *38*, L12102, doi:10.1029/2011GL047898.
- Liu, H., H. Jin, Y. Miyoshi, H. Fujiwara, and H. Shinagawa (2013), Upper atmosphere response to stratosphere sudden warming: Local time and height dependence simulated by GAIA model, *Geophys. Res. Lett.*, *40*, 635–640, doi:10.1002/grl.50146.
- Liu, H., Y. Miyoshi, S. Miyahara, H. Jin, H. Fujiwara, and H. Shinagawa (2014), Thermal and dynamical changes of the zonal mean state of the thermosphere during the 2009 SSW: GAIA simulations, *J. Geophys. Res. Space Physics*, *119*, 6784–6791, doi:10.1002/2014JA020222.
- Liu, H.-L. (2014), WACCM-X simulation of tidal and planetary wave variability in the upper atmosphere, in *Modeling the Ionosphere-Thermosphere System*, edited by J. Huba, R. Schunk, and G. Khazanov, John Wiley, Chichester, U. K., doi:10.1002/9781118704417.ch16.
- Liu, H.-L., W. Wang, A. D. Richmond, and R. G. Roble (2010), Ionospheric variability due to planetary waves and tides for solar minimum conditions, *J. Geophys. Res.*, *115*, A00G01, doi:10.1029/2009JA015188.
- Manney, G. L., M. J. Schwartz, K. Krüger, M. L. Santee, S. Pawson, J. N. Lee, W. H. Daffer, R. A. Fuller, and N. J. Livesey (2009), Aura Microwave Limb Sounder observations of dynamics and transport during the record-breaking 2009 Arctic stratospheric major warming, *Geophys. Res. Lett.*, *36*, L12815, doi:10.1029/2009GL038586.
- Matsuno, T. (1971), A dynamical model of the stratospheric sudden warming, *J. Atmos. Sci.*, *28*, 1479–1494.
- Pancheva, D., and P. Mukhtarov (2011), Stratospheric warmings: The atmosphere-ionosphere coupling paradigm, *J. Atmos. Sol. Terr. Phys.*, *73*, 1697–1702.
- Pedatella, N. M., et al. (2014a), The neutral dynamics during the 2009 sudden stratosphere warming simulated by different whole atmosphere models, *J. Geophys. Res. Space Physics*, *119*, 1306–1324, doi:10.1002/2013JA019421.
- Pedatella, N. M., H.-L. Liu, F. Sassi, J. Lei, J. L. Chau, and X. Zhang (2014b), Ionosphere variability during the 2009 SSW: Influence of the lunar semidiurnal tide and mechanisms producing electron density variability, *J. Geophys. Res. Space Physics*, *119*, 3828–3843, doi:10.1002/2014JA019849.
- Picone, J. M., A. E. Hedin, D. P. Drob, and A. C. Aikin (2002), NRLMSISE-00 empirical model of the atmosphere: Statistical comparisons and scientific issues, *J. Geophys. Res.*, *107*(A12), 1468, doi:10.1029/2002JA009430.
- Qian, L., S. C. Solomon, and T. J. Kane (2009), Seasonal variation of thermospheric density and composition, *J. Geophys. Res.*, *114*, A01312, doi:10.1029/2008JA013643.
- Qian, L., A. G. Burns, S. C. Solomon, and W. Wang (2013), Annual/semiannual variation of the ionosphere, *Geophys. Res. Lett.*, *40*, 1928–1933, doi:10.1002/grl.50448.
- Qian, L., A. G. Burns, B. A. Emery, B. Foster, G. Lu, A. Maute, A. D. Richmond, R. G. Roble, S. C. Solomon, and W. Wang (2014), The NCAR TIE-GCM, in *Modeling the Ionosphere-Thermosphere System*, edited by J. Huba, R. Schunk, and G. Khazanov, John Wiley, Chichester, U. K., doi:10.1002/9781118704417.ch7.
- Richmond, A. D., E. C. Ridley, and R. G. Roble (1992), A thermosphere/ionosphere general circulation model with coupled electrodynamics, *Geophys. Res. Lett.*, *19*(6), 601–604, doi:10.1029/92GL00401.
- Sasi, M. N., and L. Vijayan (2001), Turbulence characteristics in the tropical mesosphere as obtained by MST radar at Gadanki (13.5°N, 79.2°E), *Ann. Geophys.*, *19*, 1019–1025.

- Schmidt, H., G. P. Brasseur, M. Charron, E. Manzini, M. A. Giorgetta, T. Diehl, V. I. Fomichev, D. Kinnison, D. Marsh, and S. Walters (2006), The HAMMONIA chemistry climate model: Sensitivity of the mesopause region to the 11-year solar cycle and CO₂ doubling, *J. Clim.*, *19*, 3903–3931.
- Stening, R. J., J. M. Forbes, M. E. Hagan, and A. D. Richmond (1997), Experiments with a lunar atmospheric tidal model, *J. Geophys. Res.*, *102*(D12), 13,465–13,471, doi:10.1029/97JD00778.
- Uppala, S. M., et al. (2005), The ERA-40 Re-analysis, *Q. J. R. Meteorol. Soc.*, *131*, 2961–3012.
- Wang, H., T. J. Fuller-Rowell, R. A. Akmaev, M. Hu, D. T. Kleist, and M. D. Iredell (2012), Correction to “First simulations with a whole atmosphere data assimilation and forecast system: The January 2009 major sudden stratospheric warming”, *J. Geophys. Res.*, *117*, A03326, doi:10.1029/2012JA017630.
- Wang, H., R. A. Akmaev, T.-W. Fang, T. J. Fuller-Rowell, F. Wu, N. Maruyama, and M. D. Iredell (2014), First forecast of a sudden stratospheric warming with a coupled whole-atmosphere/ionosphere model IDEA, *J. Geophys. Res. Space Physics*, *119*, 2079–2089, doi:10.1002/2013JA019481.
- Walterscheid, R. L. (1981), Dynamical cooling induced by dissipating internal gravity waves, *Geophys. Res. Lett.*, *8*, 1235–1238, doi:10.1029/GL008i012p01235.
- Yamashita, C., H.-L. Liu, and X. Chu (2010), Gravity wave variations during the 2009 stratospheric sudden warming as revealed by ECMWF-T799 and observations, *Geophys. Res. Lett.*, *37*, L22806, doi:10.1029/2010GL045437.
- Yamazaki, Y., and A. D. Richmond (2013), A theory of ionospheric response to upward-propagating tides: Electrodynamic effects and tidal mixing effects, *J. Geophys. Res. Space Physics*, *118*, 5891–5905, doi:10.1002/jgra.50487.
- Yigit, E., and A. S. Medvedev (2012), Gravity waves in the thermosphere during a sudden stratospheric warming, *Geophys. Res. Lett.*, *39*, L21101, doi:10.1029/2012GL053812.
- Zhang, X., and J. M. Forbes (2014), Lunar tide in the thermosphere and weakening of the northern polar vortex, *Geophys. Res. Lett.*, *41*, 8201–8207, doi:10.1002/2014GL062103.